

ACS L-Flats for the WFC

J. Mack, R. Bohlin, R. Gilliland, R. Van Der Marel, J. Blakeslee, and G. De Marchi
August 21, 2002

ABSTRACT

The uniformity of the WFC detector response has been assessed by using multiple dithered pointings of moderately dense stellar fields. By placing the same star over different portions of the detector and measuring relative changes in brightness, local variations in the response of the detector have been measured. The original WFC laboratory flat fields produce photometric errors of ± 5 to ± 9 percent from corner-to-corner. New flat fields for 13 WFC filters have been delivered for use in the calibration pipeline. Initial results suggest the photometric response for a given star is now the same to $\sim 1\%$ for any position in the WFC field of view.

1. Introduction

The stability and uniformity of the low-frequency flat fields (L-flats) of the ACS detectors were tested for the WFC, the HRC, and the SBC in programs 9018, 9019, and 9024 respectively. This assessment was made using multiple pointings of a globular cluster, and thus, imaging a moderately dense stellar field. By placing the same star over different portions of the detector and measuring relative changes in brightness, local variations in the response of the detector have been determined. This ISR is devoted to a discussion of the WFC detector which requires the largest L-flat correction due to its large field of view. Future reports will address results from the HRC and the SBC detectors.

2. L-flat Campaign

For the WFC and HRC, the accuracy of the ground flats (see Bohlin et al., 2001) is assessed using observations of the globular cluster 47 Tucanae (NGC104). The target for the SBC is the globular cluster NGC6681. Observations with the WFC were offset from the cluster center to minimize the effects of crowding which can complicate the subtraction of the sky. The L-flat observing program is summarized in Table 1 for each ACS detector and includes the target RA and Dec, the dither step size, and the filters used for imaging.

Table 1. L-Flat Campaign.

Detector	Prop ID	Dither Step arcsec (% of FOV)	Target	RA	Dec	SDSS Filters	BVI Filters	UV Filters
WFC	9018	22" (11%)	47 Tucanae	00:22:37.20	-72:04:14.0	F775W F850LP	F435W F555W F606W F814W	
HRC	9019	6" (23%)	47 Tucanae	00:24:06.52	-72:05:00.6	F475W F625W F775W F850LP	F435W F555W F606W F814W	F220W F330W
SBC	9024	6" (23%)	NGC 6681	18:43:12.67	-32:17:26.3			F125LP F150LP

For observations in each detector and in each filter, the dither pattern consists of 9 pointings along a diagonal cross. For the WFC, the step size in X and Y is 22", while for the HRC and SBC filters the step size is 6" in each axis. Since the field size is ~200" for WFC and only ~25" for the HRC/SBC, each step is a large fraction of the detector field of view, as indicated in Table 1.

The 9-point dither pattern is illustrated in Figure 1 for the WFC observations, where the reference position is indicated as "dither 0". In the Figure 2, the size of each dither in pixels is shown with respect to the size of the WFC detector. Stars identified in the reference image are plotted as points in the center image and number approximately 5000 in each filter. The detector location for dithers 1 through 4 are indicated as dotted lines.

Figure 1: Nine-point dither pattern, projected onto the sky, for the WFC L-flat observations. Each step is ~ 22 arcsec in x and in y.

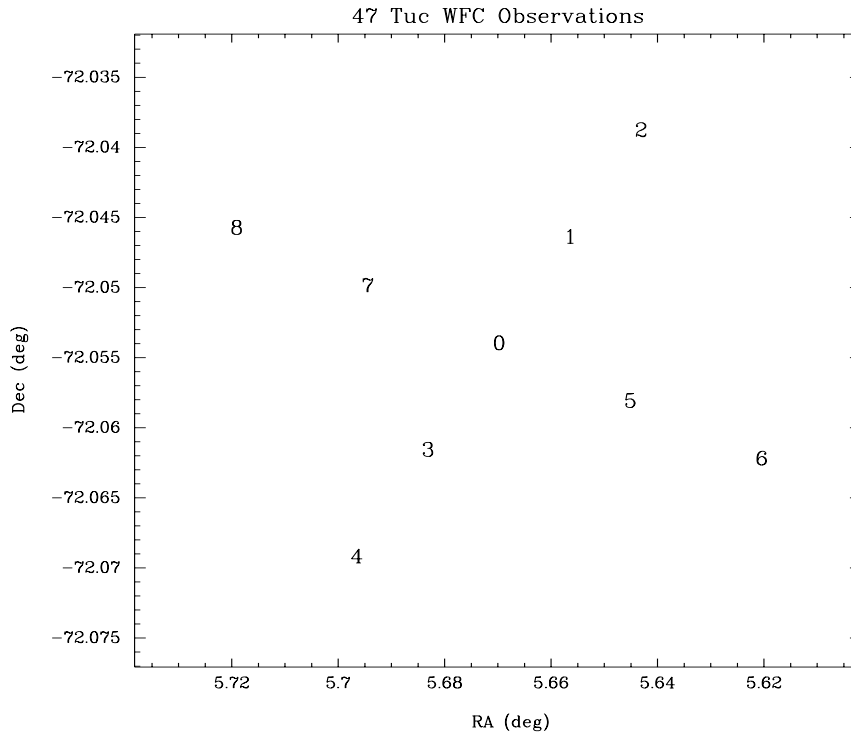
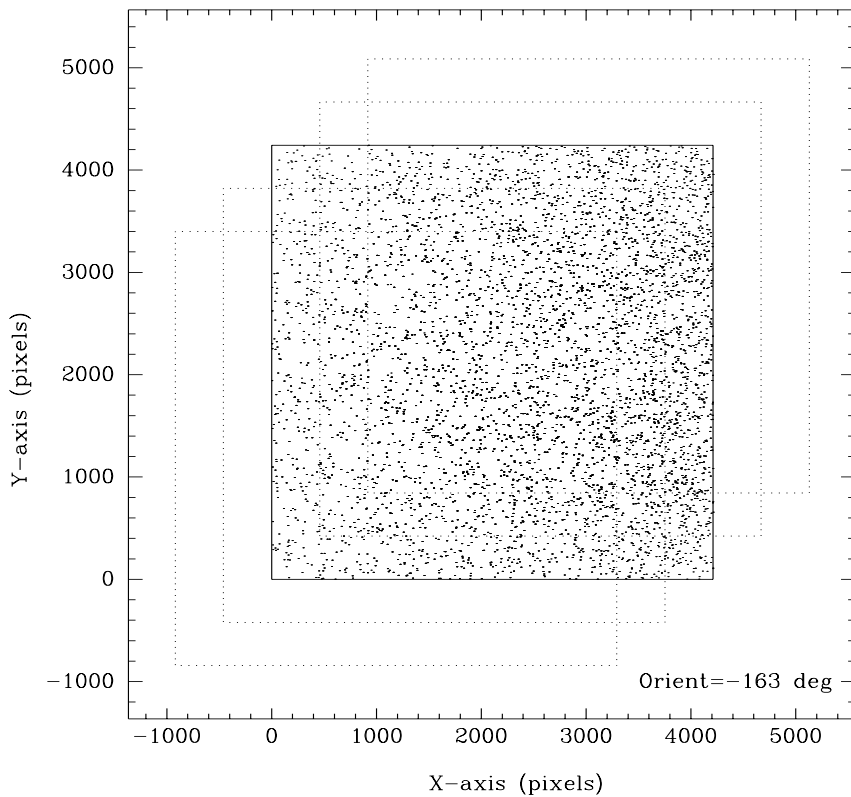


Figure 2: Nine-point dither pattern, in pixel coordinates, for the WFC L-flat observations. Each step is ~ 440 pixels in x and in y. Only dithers 0-4 are indicated in this plot.



3. WFC Observations

The WFC L-flat observations were obtained in April and May 2002. These data are summarized in Table 2. All observations, except F775W, are cr-split to avoid complications in the photometry in the presence of cosmic rays. Imaging in each filter uses a gain of 1, except for F606W, which uses gain of 2.

Due to problems with one of the gyros in April, a significant drift compromised the image quality of visits 01, 02, 11, 12, 21, 22, 31, 52, and 61. Observations for these modes were retaken in May to complete the WFC filter sample.

Table 2. WFC Filters for 47 Tuc data from program 9018.*

Filter	Visit Number	Observation Date	CR-SPLIT	Exptime	Gain
F435W	A1, A2	06 May 2002	2	60	1
F555W	B1, B2	09 May 2002	2	60	1
F606W	C1, C2	08-09 May 2002	2	45	2
F775W	51	18 Apr 2002	1	45	1
F814W	32, D1	19 Apr, 06 May 2002	2	60	1
F850LP	41, 42	18 Apr 2002	2	60	1

* Visits 01, 02, 11, 12, 21, 22, 31, 52, and 61 suffered from loss of lock due a faulty gyro.

4. Matched-Position Lists

Master coordinate lists were created by Don Lindler by applying a gaussian fit in two dimensions to each star in the reference image. Stars in each successive image were then matched with the original position list. Finally, additional stars were added which appeared in more than one dithered frame but which were not in the original reference image.

In Table 3, the coordinates derived for a single star are listed. Column 1 is the star ID number, where matching stars in different images have the same ID, and column 2 is the number of the image within the dither pattern. The third column lists the WFC chip number, and the fourth and fifth columns give the position of the star (x, y) in the calibrated image, prior to the geometric distortion correction. Because the cosmic-ray rejected, co-added images are in separate extensions for chips 1 and 2, their y-coordinates range from (1:2048) pixels for both chips. Thus, the chip ID is required for identifying stars in this reference frame. Once the data are drizzled, the distortion correction is applied and the two chips are combined into a single image, where the coordinates range from 1 to ~4200 pixels.

The geometrically corrected position (x_c , y_c) for each drizzled image is listed in columns 6 and 7. These coordinates were calculated using the coefficients of the geometric distortion solution and the measured WFC1 to WFC2 chip offset. They are accurate to within the error of the distortion solution, ~ 0.2 pixels. For example, the difference between x_c in image 0 and image 1 is equal to the dither step size in pixels. Columns 8 and 9 give the geometrically corrected position (x_{sky} , y_{sky}) of each star using image 0 as the reference frame. Note that the coordinates (x_{sky} , y_{sky}) are identical for each row to within ~ 0.2 pixels. These coordinates were derived using the measured rotation angle and slew of each image with respect to the reference image.

Table 3. Entries for star number 1 from the “Master Position List”.

star	image	chip	x	y	x_c	y_c	x_{sky}	y_{sky}
1	0	1	1598.07	3.40	1628.94	2157.12	1628.94	2157.12
1	1	1	2042.90	416.57	2085.60	2581.36	1628.80	2157.13
1	2	1	2486.33	831.63	2542.54	3005.61	1628.84	2157.20
1	3	2	1147.49	1691.44	1172.06	1733.09	1628.85	2157.27
1	4	2	698.172	1280.41	715.41	1309.18	1628.88	2157.24
1	5	2	2043.64	1627.14	2051.87	1700.87	1628.82	2157.28
1	6	2	2486.17	1157.47	2474.85	1244.44	1628.76	2157.30
1	7	1	1142.08	487.50	1205.94	2613.63	1628.77	2157.21
1	8	1	677.55	980.69	783.16	3070.23	1628.72	2157.23

5. Data Analysis

Images were calibrated using the most up-to-date bias and dark reference files. In order to eliminate cosmic-rays, pairs of cr-split images were combined using the ACSREJ routine. Flat fielding was then carried out using the LP-flats determined on the ground. If the ground-based LP-flats do not properly account for low-frequency variations, then the apparent intensity of a star will vary with dither position. We have used a least-squares solution over all stars and dithers (ISR in preparation by R. Van Der Marel) to solve for those underlying low-frequency variations.

5.1 Cosmic-Ray Rejection

Offsets between pairs of cr-split images on the order of a few tenths of a pixel can cause serious complications in the cosmic-ray rejection and image combination routine when applied to point source images. If large enough, these offsets will cause ACSREJ to incorrectly flag and reject the centers of stars, mistaking the peak of the star in the second image for a cosmic-ray. Several pairs of images in the L-flat program have been identified as having offsets of up to 0.3 pixels. These offsets could be the result of telescope “breathing”, caused by variations in temperature as HST orbits the Earth. In addition, plate scale changes between cr-split components which are separated by an Earth occultation and which are caused by differential velocity aberration can cause an overall corner-to-corner stretch of ~0.22 pixels.

In an attempt to account for registration errors between the cr-split components, the selection of the appropriate cosmic-ray elimination coefficient (*scalenoise*) has been investigated. The *scalenoise* term enters in CALACS testing via an estimate of the variance on a given pixel and consists of three terms:

$$\sigma^2 = (RN)^2 + intensity + (scalenoise \times intensity)^2$$

where: RN is the detector read noise, intensity gives a measure of the Poisson noise variance from the source plus sky, and the *scalenoise* term accounts for changes in intensity at a given pixel which may result from minor registration errors coupled with steep underlying intensity gradients for undersampled stellar images.

To analytically predict the *scalenoise* required to avoid eliminating spurious points, pairs of cr-split images with pixel offsets on the order of a few tenths of a pixel were selected. For bright stars, the first two terms in the variance equation can be ignored and $\sigma \sim scalenoise * Intensity$. To estimate the intensity for each pixel in an aperture centered on the star, the minimum value of the two exposures was taken. Then the absolute difference in intensity allows a calculation of the *scalenoise* such that 5σ is equal to the

difference pixel-by-pixel. The largest value in that aperture gives the *scalenoise* threshold for a 5-sigma test required to avoid rejecting any pixel near the bright star.

For example, the pair of cr-split images at the 7th dither position exhibit an offset of 0.3 pixels in F555W. The *scalenoise* derived using this method is approximately 0.3 or 30%, compared to the default value of 3% for the WFC. Based on the 9018 data, more than 20% of the images show registration offsets of 0.1 to 0.3 pixels. For these images, the appropriate *scalenoise* value correlates linearly with the pixel offset, i.e. a 0.15 pixel offset requires a *scalenoise* of 15%. Thus, this approach yields a direct estimate for avoiding most false eliminations of stellar peak signals at the 5-sigma level. There are, however, limitations to this approach. For a given image, a higher threshold is applied to the majority of pixels than is actually needed, thus cutting down on sensitivity to real cosmic rays. Below, we discuss this effect for our empirical *scalenoise* tests.

To empirically determine the optimal *scalenoise* for combining images, cr-split datasets were recalibrated using increasing values of *scalenoise* in the CRREJTAB reference file: the default value of 3% and larger values of 10%, 20%, 30%, and 40%. If the central pixel of a star had been incorrectly identified as a cosmic ray in one image, this pixel would have been rejected when creating the combined image, and the star would have a lower measured flux. In addition, the data quality array would show a cosmic-ray flag corresponding to the center of each star.

To determine the optimal *scalenoise* for image pairs with small offsets, aperture photometry is performed on several stars across the detector. The aperture flux derived for stars with offsets is lower when images are combined using the default *scalenoise* than when larger *scalenoise* values are used. The flux of a given star continues to increase and then level off at the best *scalenoise* value.

Table 4 summarizes these results for 3 stars in the F555W filter for dither 7 which shows an offset of 0.3 pixels. Using an aperture radius of 5 pixels, the ratio of the total flux is presented with respect to the star's "true" flux. The true flux is defined as the maximum flux derived from images which were combined using increasing *scalenoise* values. In the example shown, the best *scalenoise* is 30%, an identical result to the analytical approach. In Table 5, the same statistics are presented for the image pair at the 8th dither position, which has near-zero offset. In this case, the aperture photometry for each star produces identical results no matter which *scalenoise* is chosen.

Also presented in Tables 4 and 5 are the number of pixels flagged as cosmic rays in each image as a function of the *scalenoise* used to combine the images. The third column gives the percentage of fewer cosmic rays detected in that row versus the previous row. A larger *scalenoise* does reduce sensitivity to real cosmic rays, but this effect is less than 1% for each 10% increase in *scalenoise*.

The agreement between analytical and empirical approaches suggests that the default *scalenoise* value in the CRREJTAB reference file may not be high enough to avoid spurious data deletions, and observers should be aware of potential registration errors and the resulting impact for point source observations which are delivered from the ACS calibration pipeline.

Table 4. Empirical test to determine *scalenoise* for F555W, dither 7, where the measured (x+y) offset between cr-split pairs is 0.3 pixels and the optimal *scalenoise* is 30%.

Scalenoise (percent)	No. Cosmic Rays Detected	Percent fewer CR's	Flux Ratio Star 1	Flux Ratio Star 2	Flux Ratio Star 3
3	39616		0.925	0.907	0.903
10	30571	23%	0.970	0.960	0.977
20	25870	15%	0.983	0.971	0.998
30	24888	4%	1.000	1.000	1.000
40	24587	1%	1.000	1.000	1.000

Table 5. Empirical test to determine *scalenoise* for F555W, dither 8, where the measured (x+y) offset between cr-split pairs is 0.0 pixels and the optimal *scalenoise* is the default value of 3%.

Scalenoise (percent)	No. Cosmic Rays Detected	Percent fewer CR's	Flux Ratio Star 1	Flux Ratio Star 2	Flux Ratio Star 3
3	28501		1.000	1.000	1.000
10	28247	0.9%	1.000	1.000	1.000
20	28099	0.5%	1.000	1.000	1.000
30	27939	0.6%	1.000	1.000	1.000
40	27781	0.6%	1.000	1.000	1.000

5.2 Distortion Correction

Once the bias and dark subtraction and flat fielding are completed, the images are corrected for geometric distortion using the most recent solution derived by Don Lindler and Colin Cox. This work is documented in an ISR currently in progress. The applied IDCTAB reference table contains new fourth-order distortion coefficients for each ACS detector. A new version of PyDrizzle is required to apply the fourth-order solution and will be incorporated into the OTFR pipeline by August 21, 2002. The new IDCTAB reference files can be obtained from the archive after this date or from the ACS website at:

http://www.stsci.edu/hst/acs/analysis/reference_files/idctable_list.html

5.3 Photometry

Aperture photometry is performed for each star identified in the reference image and on its respective counterpart in the dithered images using the IRAF task **phot** in the **apphot** package. Because the matched master position lists can have errors of up to 0.2 pixels over the WFC field of view, the coordinates of each star are rederived using the intensity weighted centroid. The maximum permissible shift of the center with respect to the initial coordinate is fixed at 1 pixel.

The **phot** task assumes the data units are in DN. However, the drizzled images are in units of electrons/sec. In order to obtain the appropriate photometric errors with this task, the images are first multiplied by the exposure time and divided by the gain. Photometry is then derived for each star using an aperture of radius 5 and 7 pixels. The median sky background is computed for each star using an annulus of 7 to 11 pixels.

6. Matrix Solution

A matrix-solution program was developed by Roeland van der Marel for deriving the low-frequency flat fields from the dithered, stellar point-source photometry. Solutions for each of the five filters, F435W, F555W, F606W, F814W and F850LP, for which good cr-split data were acquired and which nicely span instrument wavelength were derived using this algorithm. The details of this code are described in a separate ISR, currently in progress.

To summarize, the observed magnitude of a star at a given dither position is assumed to be the sum of the true magnitude of the star plus a correction term that depends on the position on the detector. The correction term represents the L-flat. The L-flat, when given in magnitudes, can be expressed as the product of fourth-order polynomials in the detector x and y coordinates. When a set of multiple dithered observations is available for a given star field, the determination of both the L-flat and the instrumental magnitude of each star can be written as an overdetermined matrix equation. This equation has a unique minimum χ^2 -solution that can be efficiently obtained through singular-value-decomposition techniques. This also yields formal 1-sigma errors on the L-flat and the stellar magnitudes. Two solutions have been tested, one in which the L-flat is forced to be smooth across the chip boundary and one in which each WFC chip is treated separately. The difference between these approaches is minimal, and we have adopted the fit which is continuous across the WFC detectors.

The matrix solution requires as input the magnitude and error of each star. A 5 pixel aperture radius is chosen for the photometry since it includes ~80% of the encircled energy. Uncertainties from the sky background and from neighboring stars increase at larger radii. Sigma clipping is employed to reject stars having large photometric residuals

with respect to the variation in the L-flat. These large photometric errors are probably due to cosmic rays, image saturation, and stars falling at the detector edges.

Each WFC image contains ~5000 stars of sufficient signal-to-noise at each of the 9 dither positions. To simultaneously solve the matrix for ~45,000 unknown variables would require an enormous amount of computing time and memory. To circumvent this problem, the code was run several times on data subsamples of varying brightness. Between 3 and 5 subsamples were used, depending on filter. The results from the different subsamples always agree to <1%, and no evidence is found for dependences of the L-flat solution on stellar brightness. The final L-flat is derived from the weighted average of the individual subsets using their error frames.

To confirm that the derived L-flats are not dependent on aperture corrections, which may change across the field of view, the stellar photometry measured with a larger, 7 pixel radius aperture was also tested. The L-flat solution using photometry derived from a 5 pixel and a 7 pixel aperture agree to within 1.5 milli-mag rms. No evidence for any dependence of the L-flat solution on aperture size is found.

In Figure 3, the L-flat solutions derived for the five WFC filters are shown. The residual of the stellar magnitude with respect to the predicted magnitude is displayed, where stars in the upper left of the detector are too faint after pipeline calibration with the original ground flats, and stars in the lower right are too bright. There is a continuous gradient in the L-flat along the diagonal of the detector, which corresponds to the axis of the maximum geometric distortion. This gradient is of order 10-15% from corner to corner and is plotted in Figure 4 for each filter. The diagonal in the opposite direction shows no systematic gradient.

Figure 3: Low order flats derived for each filter from the matrix-solution code.

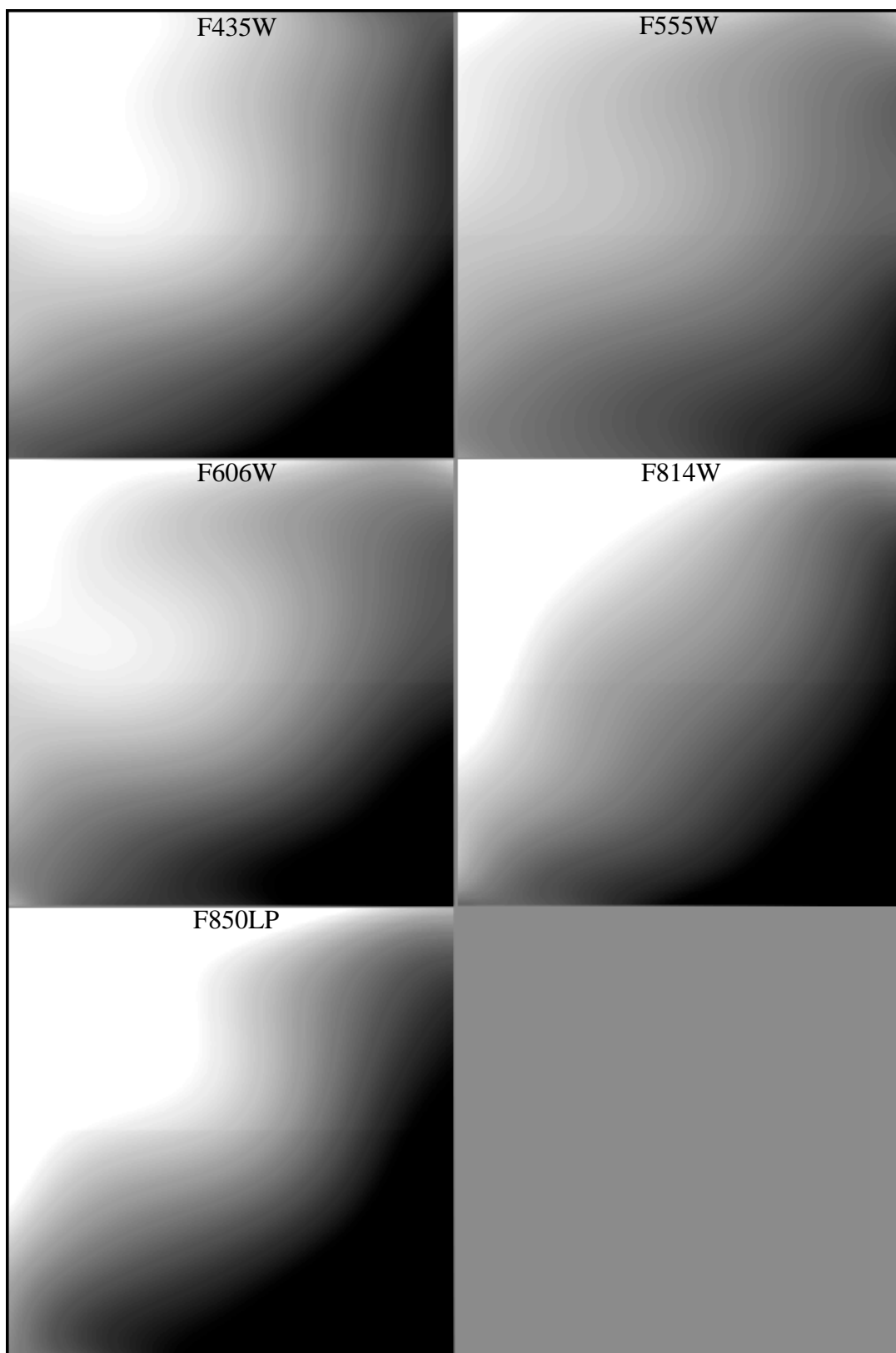
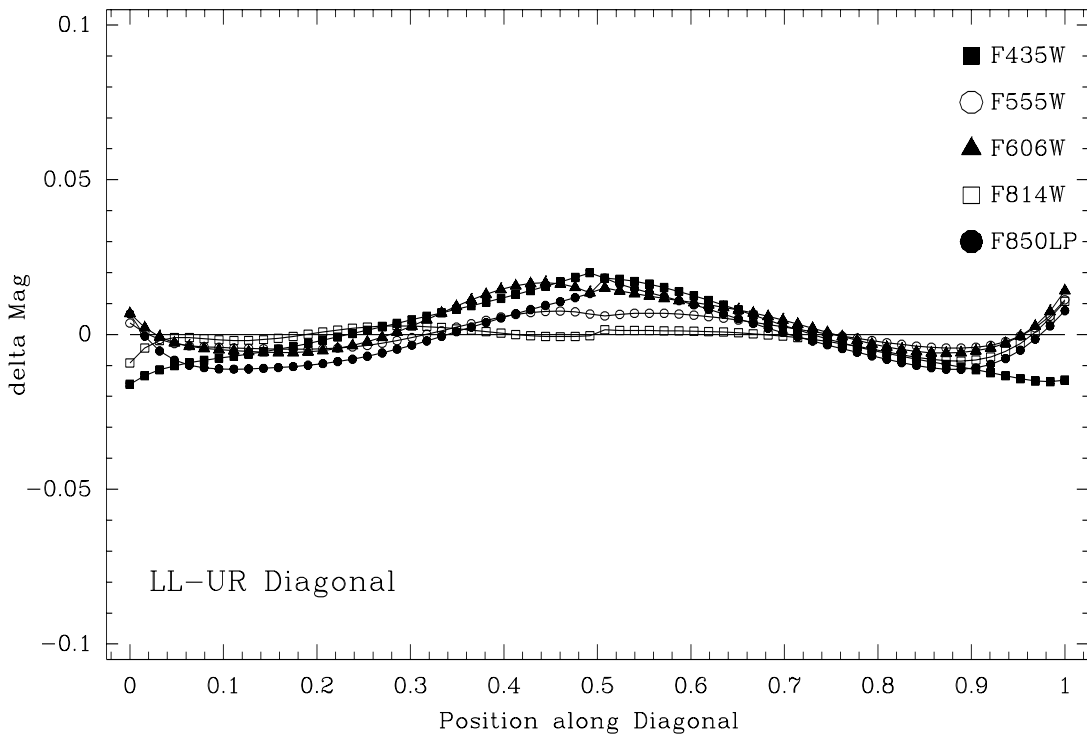
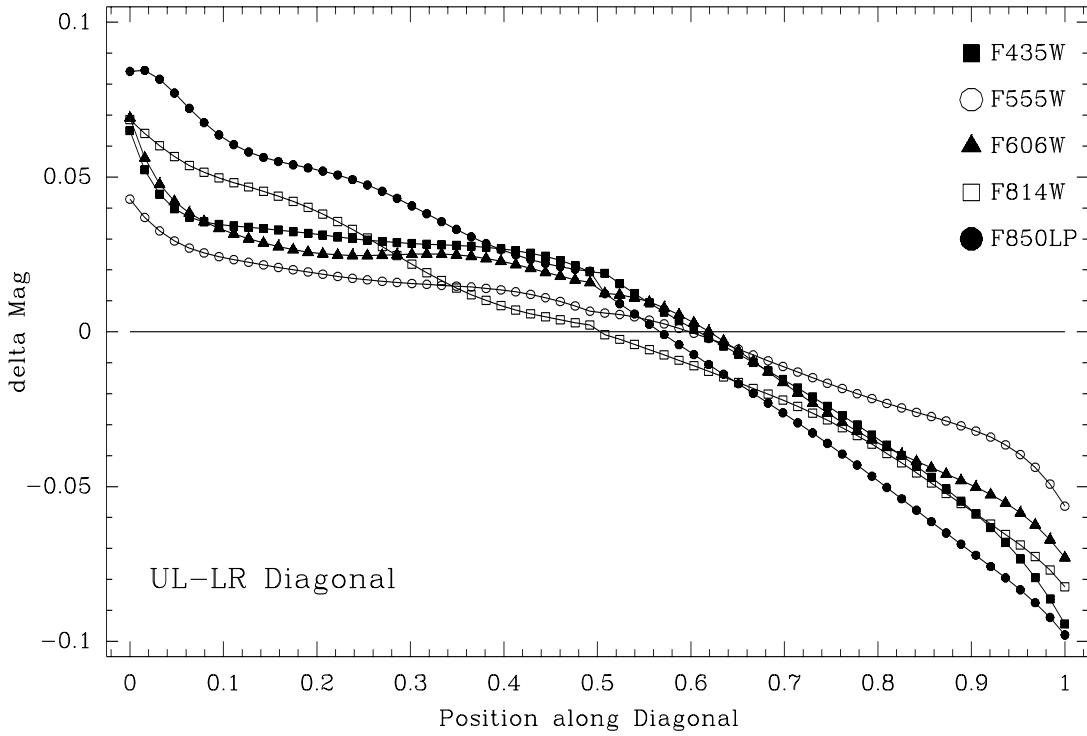


Figure 4: L-flat correction versus position along the detector diagonal. The observed gradient is along the radial direction of the Optical Telescope Assembly. Positive (negative) magnitudes indicate the photometry derived using the original ground flats is too faint (bright). The correction required to attain uniform photometry is ± 5 to ± 9 percent. The opposite diagonal shows no systematic gradient.



7. New Flat field Reference Files

The slope of the L-flat correction appears to vary as a function of wavelength, where the percent deviation along the diagonal is $\sim 18\%$ for F850LP and decreases monotonically to $\sim 10\%$ at F555W. These statistics are summarized in Table 6. Shortward of F555W, however, the slope of the correction does not follow the above trend with wavelength, but instead reverses direction.

Assuming a simple linear dependence on wavelength, the L-flat correction for the remaining wide, medium, and narrow-band WFC filters is derived. The pivot wavelength of each filter is used for the interpolation, where the resulting L-flat correction is equal to the weighted average of the L-flat correction for the two filters nearest in wavelength. This interpolation is summarized in Table 7.

Table 6. Percent variation along the upper-left to lower-right diagonal for the 5 filters analyzed in the WFC L-Flat campaign.

Filter	Pivot Wavelength	Delta Mag along diagonal (Upper Left...Lower Right) = Total
F435W	4320.3	(-0.09 ... 0.06) = 0.15
F555W	5368.6	(-0.06 ... 0.04) = 0.10
F606W	5925.3	(-0.07 ... 0.07) = 0.14
F814W	8092.4	(-0.08 ... 0.07) = 0.15
F850LP	9134.3	(-0.10 ... 0.08) = 0.18

Table 7. Weighted wavelength interpolation used to create L-flats for filters not directly observed in the WFC L-Flat campaign. The filter name in the interpolation relation refers to the L-flat correction for that filter.

Filter	Pivot Wavelength	L-Flat Interpolation
F475W	4752.5	$0.59 * F435W + 0.41 * F555W$
F502N	5022.5	$0.33 * F435W + 0.67 * F555W$
F550M	5583.4	$0.61 * F555W + 0.39 * F606W$
F625W	6307.1	$0.82 * F606W + 0.18 * F814W$
F658N	6584.1	$0.70 * F606W + 0.30 * F814W$
F660N	6599.5	$0.69 * F606W + 0.31 * F814W$
F775W	7704.5	$0.18 * F606W + 0.82 * F814W$
F892N	8915.3	$0.21 * F814W + 0.79 * F850LP$

For use in the ACS calibration pipeline, a new set of flat field reference files have been created. We have decided not to carry a separate delta-flat or L-flat, which would be multiplied by the original ground flat within CALACS. Instead, the new files are revised LP-flats and are derived by dividing the original P-flats taken on the ground by the derived L-flat corrections. These flats are renormalized to unity at the center of chip1.

The original laboratory flat fields induce photometric errors of ± 5 to 9% from corner-to-corner for the WFC. As of August 06, 2002, new flat fields for 13 WFC filters will be used during On-The-Fly-Recalibration. Any data taken prior to this date will need to be recalibrated with the flats listed in Table 8. The photometric response for a given star is now the same to $\sim 1\%$ for any position in the WFC field of view.

For delivery to the calibration database system, the order of the fits file extensions in the flat fields has been changed to match the order of the extensions in the science data. Thus, chip 2 corresponds to extensions 1-3 in the flat field and chip 1 corresponds to extensions 4-6. The header keyword *extver* remains 2 for chip 1 and 1 for chip 2.

Table 8. New WFC flat field reference files.

Filter	PFLTFILE Reference File
F435W	m820832ej_pfl.fits
F475W	m820832fj_pfl.fits
F502N	m820832gj_pfl.fits
F550M	m820832hj_pfl.fits
F555W	m820832ij_pfl.fits
F606W	m820832jj_pfl.fits
F625W	m820832kj_pfl.fits
F658N	m820832lj_pfl.fits
F660N	m820832mj_pfl.fits
F775W	m820832nj_pfl.fits
F814W	m820832oj_pfl.fits
F850LP	m820832pj_pfl.fits
F892N	m820832qj_pfl.fits

8. WFC Sky Flats

Analysis of the ACS/WFC EROs and early science images showed an obvious gradient in the sky background of each filter on the order of 10%. These images were flat-fielded using the ground flats and showed the sky to be faintest in the upper left corner of the detector and brightest in the lower right corner. Prior to the availability of the photometric L-flats, the ACS IDT removed this observed gradient by fitting low-order polynomials to the sky background.

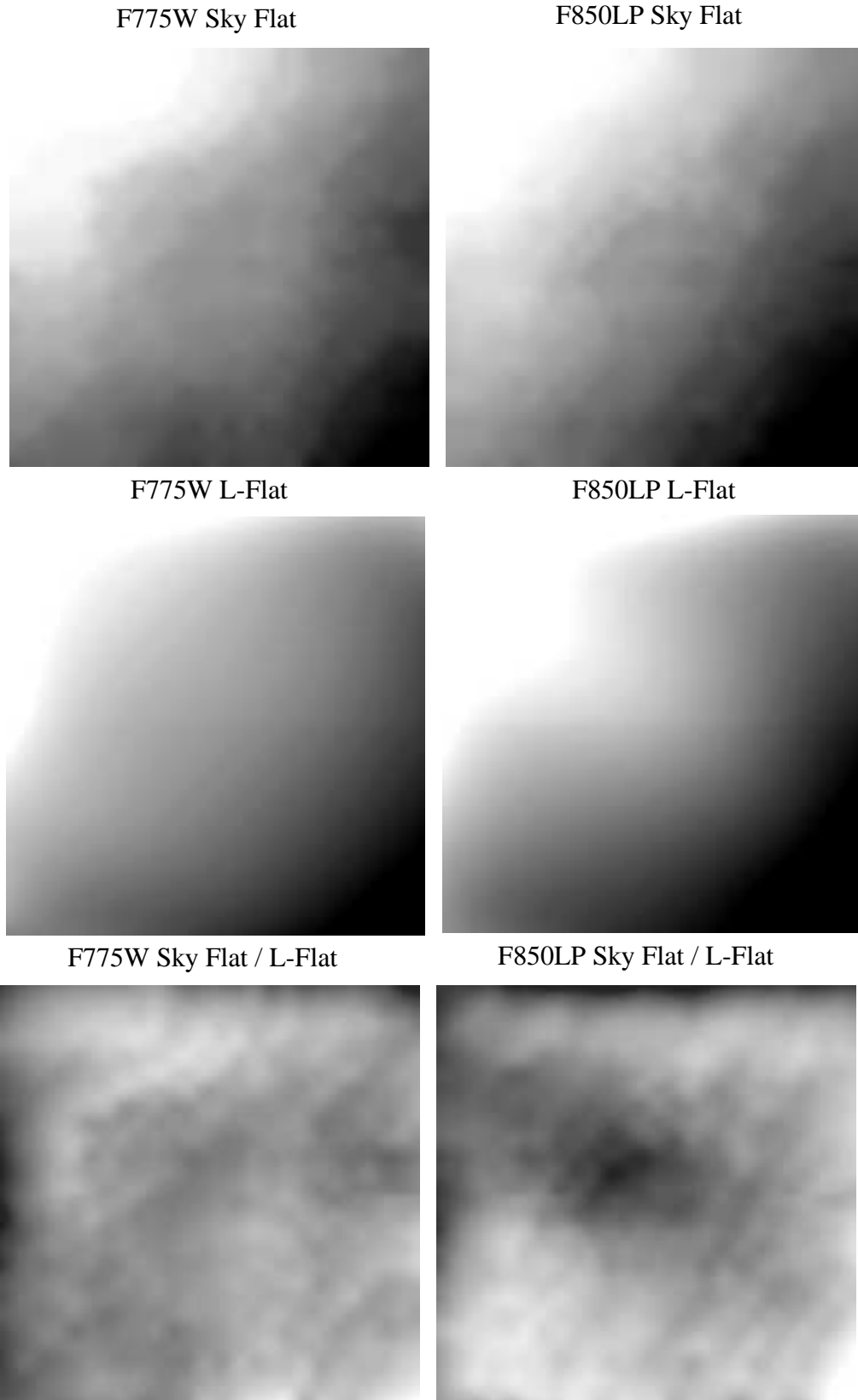
For comparison with the L-flats derived from point source photometry, sky flats were created by John Blakeslee using high signal-to-noise exposures of the Hubble Deep Field-North which contains a relatively large amount of “blank” sky. For F775W and F850LP, the combined exposures are 4500 sec and 6800 sec, respectively. SExtractor is used to fit a smooth, low-order bicubic spline to the sky background, after first masking all detected sources. The resulting image is then normalized by its mean countrate to produce the sky flat field.

The similarity between the L-flat and sky flat solutions in Figure 5 is rather striking. Both show a variation which is correlated with distance along the upper-left to lower-right diagonal. The ratio of the F775W sky flat to the photometrically derived L-flat shows residuals of order 1%, which are relatively flat across the detector. The F850LP residual, on the other hand, shows ~2% deviation at the center of the detector, corresponding to the black region at the center of the lower-right image. This region is the central “blob” blemish described in Bohlin et al. (2001 and 2002), which exhibits the largest changes in flat field structure with wavelength. This effect is illustrated in Figure 8 of Bohlin et al. (2002), which compares the broadband to monochromatic flats at long wavelengths. The ratio of these long wavelength flats shows a central “blob” and surrounding ring with errors of $\pm 2\%$.

Uncertainties in the sky flat field are dependent on the accuracy of the bias subtraction. If the bias level is off by a constant, then the residual image would look like the inverse of the applied flat field. Alternately, the observed L-flat to sky flat residual could be caused by differences in color between the sky spectrum and the globular cluster stars. However, L-flats derived using only the bluest stars near the cluster turnoff and only the reddest stars at the bottom of the main sequence do *not* show differences which resemble the F850LP residual. The change of stellar spectra across the F850LP bandpass is, however, relatively small in these data for a sensitive test.

As more precise, high signal-to-noise sky flats become available over the next few months, detailed comparisons with L-flat solutions from the 47 Tuc data will be possible, with the anticipated redelivery of improved flat fields.

Figure 5: F775W and F850LP Sky Flat, L-flat, and residual. The gradient along the diagonal is $\pm 7\%$ and $\pm 9\%$ for each filter, respectively. The residuals are $\pm 1\%$ and $\pm 2\%$.



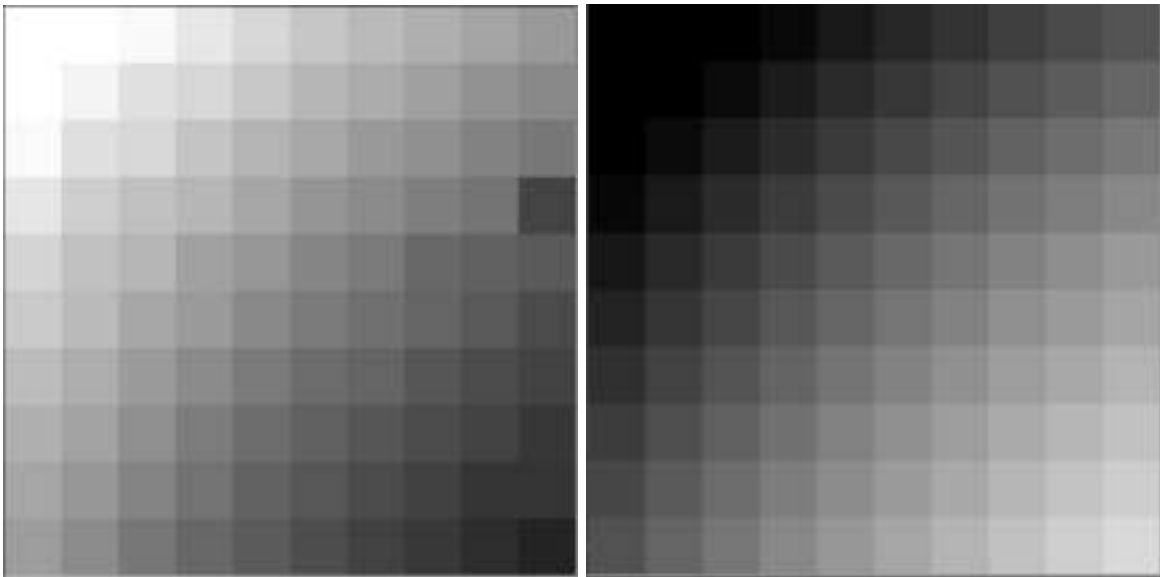
9. Distortion Correction Verification

The gradient in both the L-flat and sky flat images is along the diagonal of the detector corresponding to the axis of maximum geometric distortion. Thus, it is important to verify that the observed gradient is not caused by an inadequate distortion solution or by an error in PyDrizzle when implementing this solution.

To verify the distortion solution, aperture photometry is performed for each star before and after the geometric distortion correction. Using the standard 5 pixel radius aperture, measurements are taken in the calibrated, cosmic-ray rejected images (**crj.fits*) and in the distortion corrected images (**drz.fits*). For ease of comparison, the WFC field of view is divided into a 10x10 grid based on the star (x, y) coordinates in the calibrated image, prior to the distortion correction. Then, the sum of the flux for all stars falling within a given bin is determined for both the **crj.fits* and **drz.fits* images. This effectively gives the weighted intensity average of all the stars. Finally, the ratio of the flux in each bin is calculated and is plotted in Figure 6a.

To verify the distortion correction, this ratio is compared with the variation of the WFC effective pixel area with position. The pixel area map shown in Figure 6b corresponds to Figure 4.3 (binned 10x10) in the ACS Data Handbook and is derived from the geometric distortion solution. The scale in Figure 6 is 1.10 (white) to 0.93 (black). If the distortion correction had been applied appropriately, these images would be the direct inverse of one another, which is true to ~1%.

Figure 6: a.) Weighted-average flux ratio of stars in a 10x10 grid measured before and after the geometric distortion correction. b.) Variation of WFC effective pixel area with position derived using the fourth-order distortion correction.



10. WFC Sensitivity Analysis

The initial ACS sensitivity program (proposal 9020) observed the same star (GD71) at the center of WFC1 and WFC2 in April 2002. Preliminary analysis of the sensitivity, based on the pre-launch flat field frames, showed discrepancies between the two WFC chips of up to ~8%, with a mean ratio of 1.030 ± 0.008 . These discrepancies were expected to disappear once the appropriate L-flat corrections had been made.

In July and August 2002, a second sensitivity calibration program (proposal 9563) observed the star GRW+70D5824. A comparison of the sensitivity derived from measurements of GD71 and of GRW+70 indicates that the two stars agree to within 1%.

Once the new L-flat solutions were derived, all sensitivity observations were re-processed using the new LP-flats. Discrepancies which were previously found between the two chips are now less than 1%, and the mean ratio becomes 1.005 ± 0.004 . Table 8 presents the ratio of the countrate in chip 2 to chip 1 using a 2.5" aperture radius for each wide-band filter and compares the chip ratio before and after the L-flat correction.

Table 9. WFC2/WFC1 Sensitivity ratio prior to and after L-flat correction. The target used for calibration is listed in parentheses.

Filter	WFC2/WFC1 Pre- L-Flat Correction (GD71)	WFC2/WFC1 Post- L-Flat Correction (GD71+GRW70)
F435W	1.078	1.027
F475W	1.005	0.985
F555W	1.019	1.002
F606W	1.022	1.005
F625W	1.025	1.004
F775W	1.014	1.007
F814W	1.028	1.004
F850LP	1.048	1.007
Average	1.030 ± 0.008	1.005 ± 0.004

11. L-flat Verification Using 47 Tuc Color-Magnitude Diagrams

To verify the photometry derived after the L-flat correction is applied, features in the color magnitude diagram for 47 Tucanae are examined. More than 3500 stars were matched in the F435W, F555W and F814W filters, from one magnitude above the cluster turnoff to four magnitudes down the main sequence. Zero points were added to each band-pass to approximately match the position of the 47 Tuc color-magnitude diagram (CMD) from numerous published sources using standard Johnson-Cousins B, V, and I photometry.

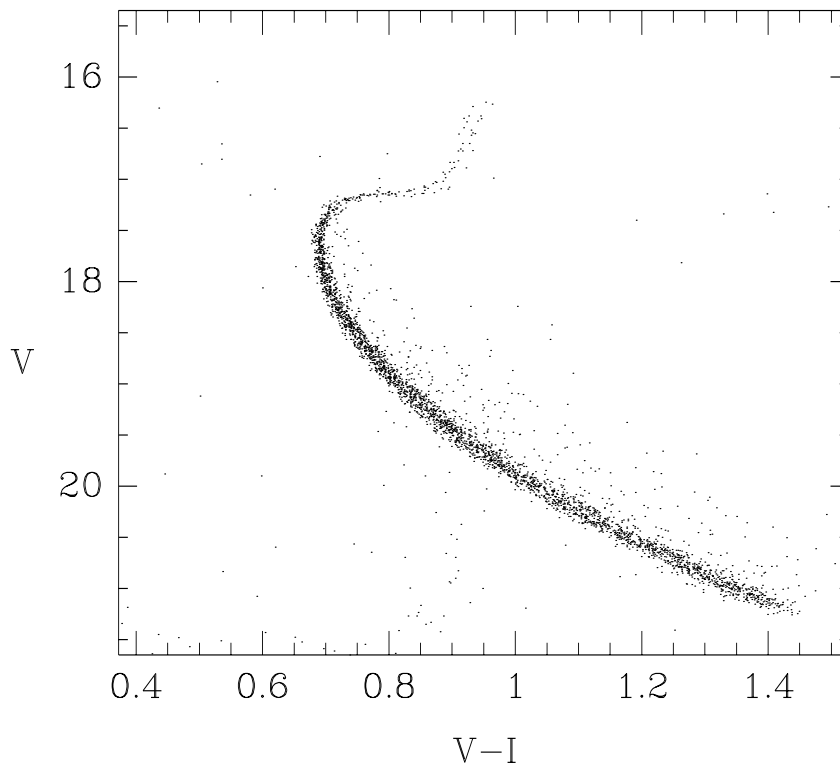
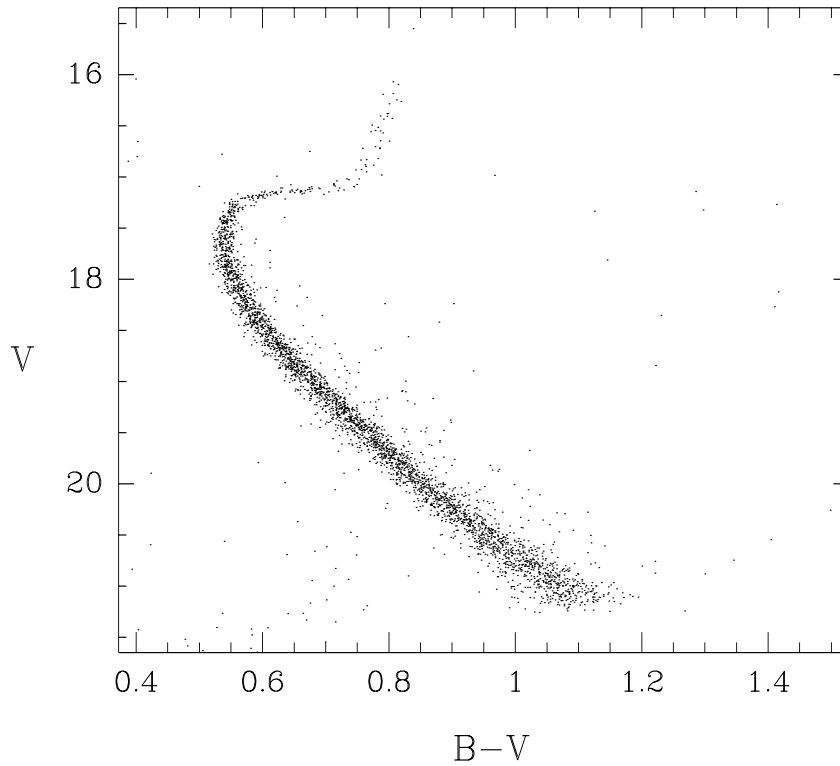
In Figure 7, the V vs. B-V and V vs. V-I color magnitude diagrams are shown. The relevant comparison is not the consistency of the zero points (which are arbitrary for this test), but rather the consistency of CMD features for stars observed over different portions of the detector. In particular, the L-flat corrections are largest in the upper-left and lower-right corners, so it is natural to consider whether CMDs for these regions are consistent.

The nearly horizontal CMD region, which is associated with the transition to sub-giants, can be used to test for any positional dependence. Twenty stars were selected from each corner of the 47 Tuc image for the region near $V = 17.15$ in the CMD. The difference in V magnitude measured between the upper-left and lower-right corners is only 0.001 ± 0.006 mag for regions which are separated by more than 2000 pixels along the diagonal. A test along the opposite diagonal gives a similarly small change.

The nearly vertical CMD region near $V = 17.7$, which is associated with stars nearing the main sequence turnoff, can be used to check for positional dependencies in B and I relative to V. These tests confirm that the photometry is consistent to within a few milli-magnitudes over the chip.

Photometry using the new LP-flats for 47 Tuc in the B, V, and I bands yield excellent CMDs (the ACS CMDs are noticeably tighter than CMDs published from much more extensive WFPC2 observations within the same field). These results confirm that any field dependence in the point source photometry, caused by inaccurate flat fields, geometric distortion effects, and aperture corrections, has now been corrected for.

Figure 7: Color magnitude diagrams for 47 Tuc derived from B, V, and I photometry after applying the L-flat correction. Each WFC exposure is 60 seconds. A precise transformation to the standard B, V, I system has not been attempted, and small color terms may be unaccounted for in these plots.



12. Future Analyses

The remaining L-flat data to be analyzed from program 9018 consists of non- CR-SPLIT exposures for the WFC in filter F775W. The HRC data taken in program 9019 are also not CR-SPLIT, with the exception of the UV filters. The least squares L-flat solution for these cases will need to be modified to flag outliers as a means of controlling against cosmic rays. Analysis of the SBC flat fields will follow analysis of the HRC.

Recommendations

The original ground flats require corrections of ± 5 to ± 9 percent. The current flats are now accurate to ± 1 percent. Additional corrections could reduce the errors to $\sim 0.5\%$. Observers are encouraged to check the latest ACS Flat field reference files available for recalibration. The files can be found at the ACS website:

http://www.stsci.edu/hst/acs/analysis/reference_files/flatimage_list.html

References

- Bohlin, R.C., Hartig, G., & Martel, A. 2001, Instrument Science Report, ACS 01-11, (Baltimore:STScI).
- Bohlin, R.C. & Hartig, G. 2002, Instrument Science Report, ACS 02-04, (Baltimore:STScI).

Acknowledgements

We would like to thank the ACS Calibration and Photometry Working Group for valuable brainstorming sessions related to this work. We also express thanks to Don Lindler for creating the matched-position lists, Gehrhardt Meuer for useful comments and suggestions, Colin Cox for input on velocity aberration, and Tom Brown for sharing his insights on creating L-flats for STIS.